Technical Sciences, 2018, 21(4), 303–321

UNIWERSYTET WARMIŃSKO-MAZURSKI W OLSZTYNIE

Quarterly peer-reviewed scientific journal
ISSN 1505-4675
e-ISSN 2083-4527
TECHNICAL SCIENCES
Homepage: www.uwm.edu.pl/techsci/

IMPACT OF FRICTION COEFFICIENT ON PARTICLES CIRCULATION VELOCITY CALCULATED BY EULER-LAGRANGE MODEL IN SPOUTED BED APPARATUS FOR DRY COATING

Wojciech Ludwig

Department of Chemical Engineering
Faculty of Chemistry
Wroclaw University of Technology

Received 14 May 2018; accepted 20 November 2018; available online 21 November 2018.

K e y w o r d s: spout-fluid bed, friction coefficient, restitution coefficient, Euler-Lagrange approach.

A b s t r a c t

This paper is a continuation of research concerning gas-solid flow modelling using the Euler--Lagrange approach in a spout-fluid bed apparatus. The major challenge in this case was to determine the friction coefficient for particles hitting against the walls of the apparatus. On the basis of the properties of similar materials the value of this quantity was estimated at 0.2. Therefore, it proved useful to check the model's sensitivity to the value of this parameter. The study investigated the effect of friction coefficient on calculated values of particles velocity in the draft tube and the annular zone of the device for various volumes of the circulating bed. In the course of calculations, a relatively small influence of friction coefficient on particles velocity was observed in the tested zones of the apparatus. The changes were most visible for large volumes of the bed, which was connected with an increase in the number of collisions of particles with the walls.

Symbols

a – coefficient of Morsi-Alexander drag law, –,
a_s – particle acceleration, m/s^2,
c – coefficients of e_t correlation, –,
C_D – drag coefficient, –,
d – particle diameter, m,

Correspondence: Wojciech Ludwig, Zakład Inżynierii Chemicznej, Wydział Chemiczny, Politechnika Wrocławska, ul. Norwida 4/6, 50-373 Wrocław, e-mail: wojciech.ludwig@pwr.edu.pl

e – restitution coefficient, –,
E^* – effective Young's modulus for impact of two materials, Pa,
$F_{\text{interaction}}$ – averaged force of momentum exchange between phases per unit volume, N/m^3,
$F_{\text{exchange},i}$ – force of momentum exchange between fluid and individual particle per unit mass, N/kg,
g – gravitational acceleration, m/s^2,
H – height of the fixed bed, m
I – unit vector
m – mass, kg.
m^* – effective mass for impact of two materials, Pa,
P – pressure, Pa,
R^* – effective radius for impact of two materials, m
Re – relative Reynolds number, –,
S_g – deformation rate tensor of fluid phase
u_g – velocity vector of fluid phase, m/s
$u_{s,i}$ – velocity vector of individual solid particle, m/s
V – velocity component, m/s, volume, m^3,
w – average velocity, m/s
x – coordinate vector (x, y, z)

Greek letters

β – momentum transfer coefficient, –
η – dynamic viscosity of the fluid, Pa·s,
θ_i – incident angle according to Wu et al. (2007),
$(\theta_i)_{\text{Fluent}}$ – incident angle according to ANSYS Fluent software, °,
Θ – nondimensional angle of incident, –,
Θ_{crit} – critical value of nondimensional angle Θ, –,
κ – rigidity coefficient, –,
λ – kinetic energy loss ratio, –,
μ – friction factor, –,
ρ – density, kg/m^3,
τ_g – stress tensor of fluid phase
ω – volume fraction, m^3/m^3.

Subscripts

bed bed
elast elastic
g gas
i incident
n normal
o inlet
r rebound
s solid
t tangential
Thornton from Thornton's model
y yield

Introduction

Spouting apparatuses were created as a modification of classic fluidized bed devices (MATHUR, GISHLER 1955). They eliminated their basic disadvantage, i.e. the possibility to use only small particles (SUTKAR et al. 2013). They enabled operations on beds of materials with diameters of up to several millimetres (Geldart's class *D*) (GELDART 1973). This is related to the unique characteristics of the bed flow in such devices (EPSTEIN, GRACE 2011, MOLINER et al. 2017). The gas, which is fed only through the hole in the axis of the device, lifts the particles in the so-called spout zone. Then they form a spout above the surface of the bed and fall freely into the annular zone (annulus), where they are entrained again to the spout zone. Taking into account the movement of particles, the two zones differ considerably. In the central part, we are dealing with pneumatic transport, high flow velocities of both phases and a small volume fraction of solids. On the contrary, in the annular zone, a slowly moving packed bed is created. Due to this mode of operation the spouting devices have been used from the very beginning in many areas of the economy (EPSTEIN, GRACE 2011, MOLINER et al. 2017). Spouting is widely used for drying sticky materials, e.g. pastes, sludge and grains with high moisture content, and in the food industry for dehydrating fruit and vegetables. This type of devices is also used for pyrolysis, combustion and gasification of waste materials, e.g. biomass, post-production sludge, used plastics and tyres. The ordered movement of particles compared to the fluidized bed makes the spouting devices ideal for coating in both the pharmaceutical and food industries (TEUNOU, PONCELET 2002). A coating layer is applied in the spout zone and the material is dried in the annular zone. In classic spouting devices, particles are entrained into the spout zone from any point in the annular zone, which results in varying humidity and a random distribution of the coating times (ZHONG et al. 2010). The solution to this problem is the use of the draft tube that physically separates the two zones and thus organises the circulation of particles. They may only be entrained into the spout zone along a short distance between the lower edge of the tube and the bottom. In addition, the draft tube reduces the minimum spouting velocity and allows the use of high beds (no maximum spoutable bed depth) (ISHIKURA et al. 2003).

Initially, the coating was carried out in spouting apparatuses where the spray nozzle was located in the upper part of the chamber with the bed. However, both the efficiency of the process and the quality of the coating were low. Therefore, devices with a spraying nozzle located in the lower part of the bed have been introduced. In this system, the probability of collision between the particles and the coating droplets is higher and the drying time shorter, however, there is a risk of agglomeration of moistened bed particles due to their high concentration just above the nozzle. This can be prevented by using an additional stream of fluidizing air (spout-fluid bed system). Some modification of the construction

described above is the Wurster apparatus – a spout-fluid device with the draft tube and a nozzle in the bottom. It is considered to be the best design for coating of fine grain materials (TEUNOU, PONCELET 2002, KARLSSON et al. 2006).

SZAFRAN et al. (2012) presented a new spout-fluid device with internal bed circulation, which is a modification of the Wurster apparatus, in which the hydrodynamics of particle flow significantly differs from that of classic spout apparatus. Thanks to the significant elongation, the device operates in the fast circulating dilute bed regime, which is characterized by low concentrations of particles in all zones and their high speed (LUDWIG, ZAJĄC 2017). Therefore, the device is suitable for dry powder coating of materials with small grain size, even those in Geldart's Group C (GELDART 1973).

The correct description of phase flow hydrodynamics is the basis for modelling the coating process in the spouting apparatuses. Due to the intensive development of models describing multiphase flows, computational algorithms and the increase in power of computer hardware, an increasing role of computational fluid dynamics (CFD) in the modelling of spouted beds can be observed. In the case of gas-solid systems, there are two approaches: Euler-Euler (EE) and Euler-Lagrange (EL) (RANADE 2002, MOLINER et al. 2017). The first approach treats both phases as interpenetrating continua. Equations describing both phases have a similar structure, they differ only in the volume fraction of a given phase (RANADE 2002). They are solved for each phase separately. We take into account the interaction of phases through pressure and the terms called interphase coefficients of momentum, energy and mass exchange (LUDWIG, ZAJĄC 2017). EE models have no limitations concerning volume fraction of individual phases; they can be used in devices of any scale. Unfortunately, in their case it is necessary to develop a model describing the rheology of the dispersed phase. EE models do not provide accurate information on particle movement – we only know their volume fraction and average velocity. The calculation cost of these methods is low, so they are often used. In this case, however, it is necessary to validate the values of the model parameters, e.g. packing limit, restitution coefficient, etc. (LUDWIG, ZAJĄC 2017). These must be determined by comparing the results of the simulation with the experimental data for a given device. In relevant literature there is a lack of satisfactory data, e.g. for devices with circulating bed.

EL models describe the dynamics of the continuous phase using the cell averaged momentum transport equations (DEEN et al. 2007). The motion of the dispersed phase is modelled by solving motion equations for each of its elements individually, which entails a high demand for computational power and memory (JAWORSKI 2005). Fluidized and spouted beds are characterized by granular flows with a high volume fraction of the dispersed phase. Therefore, in EL approach such flows are most often described using DEM (Discrete Element Method) (CUNDALL, STRACK 1979). In its original form, it is insufficient to describe

the multiphase fluid-solid flows, as it does not take into account the hydrodynamic forces resulting from the momentum exchange between the fluid stream and the particles that move within it. In this case, the DEM method is combined with the CFD models: the dispersed phase is described using DEM and CFD models are used for the continuous phase (fluid). This CFD-DEM approach has become an effective tool to study the hydrodynamics of complex granular flows. Two approaches are used to describe interparticle and wall collisions: soft-sphere and hard-sphere. The soft-sphere method assumes that particles may experience microdeformation in the contact point area due to friction and stress (TSUJI et al. 1993). Deformations cause some strain, i.e. 'numerical' displacement of two bodies. The greater the strain, the higher the value of the contact force between the bodies. The hard-sphere method assumes that all interparticle interactions are binary and immediate (contact time is infinitely small) and that contact forces are impulsive (HOOMANS et al. 1996, WACHEM, ALMSTEDT 2003). The particles are spherical and this shape is retained after impact. The basic correlations used in this method are the balance of momentum and energy before and after the collision. The contact between the bodies is point-based and during its course they undergo normal and tangential deformations resulting from the occurring elastic forces. Particle velocities after collision are determined by the pre-collision velocities and restitution factors according to the formula:

$$e_{n,t} = \frac{V_{r\,n,t}}{V_{i\,n,t}} \tag{1}$$

When we deal with the significant low volume fraction 10^{-3}–10^{-4}, a simplified DEM model called the Discrete Phase Model (DPM) can be used to describe the circulation of the dispersed phase, where only collisions of particles with the walls of the apparatus are taken into account. During the previous studies the author presented a model of particle-wall collision, which was successfully used to calculate the velocity of particles in the key area for coating in the modified Wurster apparatus (LUDWIG, PŁUSZKA 2018). The model assumed the use of selected Thornton and Wu equations describing respectively the normal and tangential restitution coefficient as a function of the particle velocity and the angle of its incidence on the surface from which it rebounds (THORTON et al. 2001, WU et al. 2009). In order to be able to apply the model equations, it was necessary to know many physical properties of the circulating particles and the material of the walls (see Tab. 1). The biggest problem in this case was to determine the value of the friction coefficient of particles against the walls of the apparatus. Based on the properties of similar materials, its value was initially estimated at 0.2 (WU, SEVILLE 2016). In order to check the impact of an error in adopting this value on the correctness of calculating the particle velocity in the apparatus, an analysis was made of the dependence of the results

in the draft tube zone and the annular zone on the assumed friction coefficient value for various volumes of the bed. Data obtained from computer simulations were compared with experimental results.

Modelled apparatus

The modelled device is presented in Figures 1 and 2. Its main part is a very long column (3 m high) consisting of three cylindrical glass segments *B*, *D* and *E* and an aluminium cone *C* with air supply nozzles, a plasticiser and a coating substance, which, contrary to classical solutions, was placed between the lower segment *B* (particle acceleration zone) and the upper part *D* of the device (coating zone).

In the axes of the segments there is a glass draft tube 6, above which there is a metal deflector 8, which prevents the bed from being blown away and allows for the use of high velocities of spouting air. It is fed through the injector 10, which sucks the gas from the annular zone. The particles poured into the apparatus fall freely to the bottom of the lower segment B. When the spouting gas stream 1 is switched on, the particles are sucked in and accelerated to achieve the required circulation velocity, passing through cone *C* with powder nozzle 3

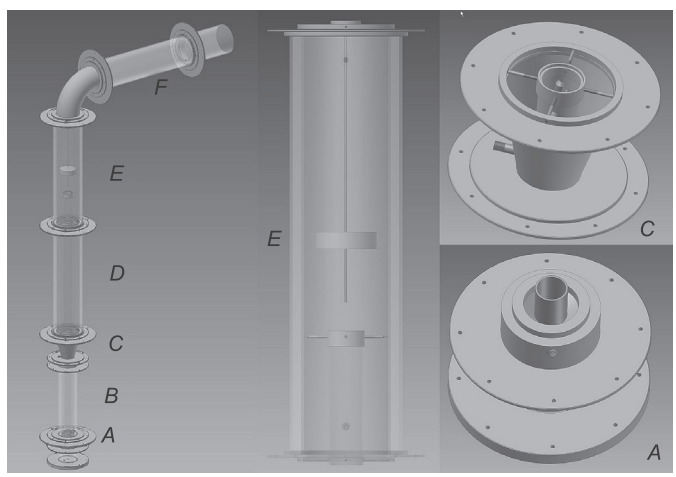

Fig. 1. Diagram of spout-fluid bed apparatus with a circulating dilute bed for dry coating: *A* – particle entrainment zone, *B* – bottom segment (acceleration zone), *C* – cone with nozzles spraying the plasticiser and coating powder, *D* – middle segment (coating zone), *E* – upper segment (spouting zone), *F* – outlet (dust extraction zone). Dimensions of the apparatus: height: 3 m, inside diameter of the lower section 0.08 m, inside diameter of the upper section: 0.15 m, length of the draft tube: 1.78 m, its inside diameter in the lower section: 0.041 m, its inside diameter in the upper section: 0.054 m
Source: based on LUDWIG and ZAJĄC (2017), LUDWIG and PŁUSZKA (2018).

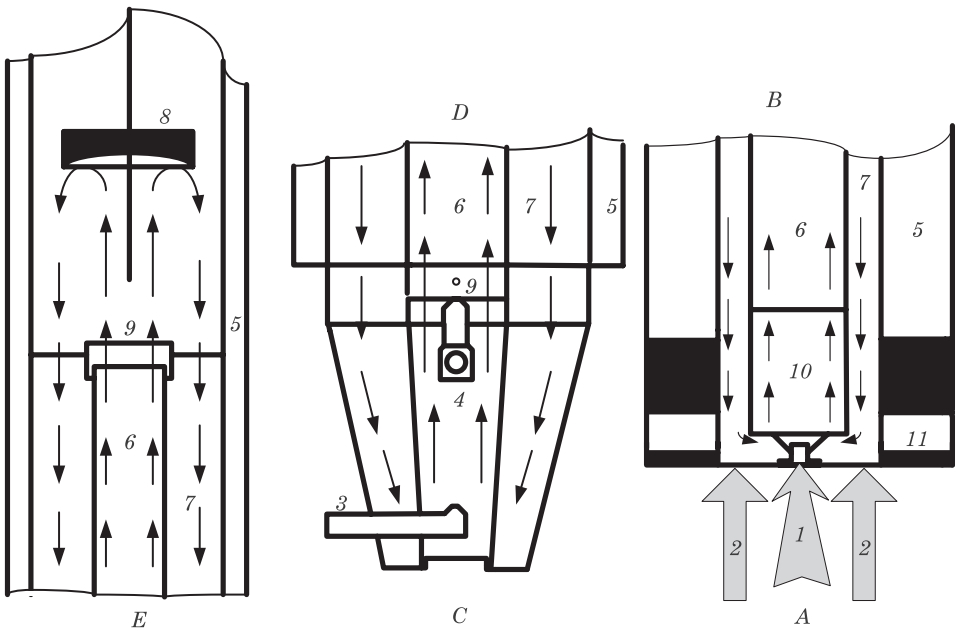

Fig. 2. Details of selected parts of the spout-fluid bed apparatus with a circulating dilute bed for dry coating (the arrows show the trajectories of the movement of the coated particles): *A* – entrainment zone with the injector, *B* – bottom segment (acceleration zone), *C* – cone with nozzles, *D* – middle segment (coating zone), *E* – upper segment (spouting zone); *1* – main stream of spouting air, *2* – stream of fluidizing air, *3* – powder spraying nozzle, *4* – plasticizer nozzle, *5* – double external glass wall of the apparatus, *6* – glass draft tube, *7* – annular zone (drying zone), *8* – aluminium deflector, 9 – aluminium connecting rings, *10* – metal injector, *11* – holes for bed unloading

Source: based on LUDWIG (2016).

and plasticiser nozzle 4, and then through the upper draft tube 6 in segment *D*. When they leave the draft tube, they rebound off deflector 8, fall into annular zone 7 and fall to the bottom. In entrainment zone *A*, they are sucked in again.

Model description

In Eulerian-Lagrangian modelling the flow of the continuous phase is described by means of the transport equations averaged in the calculation cell. A significant difference, in comparison to single-phase flows, is the inclusion of the volume fraction of the phase ω in the equation terms. The continuity equation is in the form (WACHEM, ALMSTEDT 2003):

$$\frac{\partial}{\partial t}\left(\omega_g \rho_g\right) + \nabla\left(\omega_g \rho_g u_g\right) = 0 \tag{2}$$

where the index g means the continuous phase (fluid). The momentum conservation equation:

$$\frac{\partial}{\partial t}\left(\omega_g \rho_g \boldsymbol{u_g}\right) + \nabla\left(\omega_g \rho_g \boldsymbol{u_g} \boldsymbol{u_g}\right) = -\omega_g \nabla P + \nabla\left(\omega_g \boldsymbol{\tau_g}\right) + \omega_g \rho_g \boldsymbol{g} + \boldsymbol{F}_{\mathbf{interaction}} \quad (3)$$

contains a stress tensor $\boldsymbol{\tau_g}$ defined as:

$$\tau_g = 2\eta S_g - \frac{2}{3}\eta S_g^T I \quad (4)$$

where η is the dynamic viscosity of the fluid, $\boldsymbol{I}$ is the unit vector, and $\boldsymbol{S_g}$ is the tensor of the deformation velocity in the continuous phase:

$$S_g = \frac{1}{2}\left(\nabla u_g + \left(\nabla u_g\right)^T\right) \quad (5)$$

In equation (3), the source term $\boldsymbol{F}_{\mathbf{interaction}}$ represents the average effect of the momentum exchange between the continuous phase and all the elements of the discrete phase that are present in the control volume under investigation:

$$F_{\text{interaction}} = \frac{\sum_{i=1}^{N}\left[V_{s,i}\rho_s F_{\text{exchange, i}}\right]}{\sum_{i=1}^{N} V_{s,i}}\ \delta \quad (6)$$

In equation (6), $V_{s,i}$ is the volume of the i-th solid particle and δ is a pulsating function:

$$\delta = f\left(\boldsymbol{x_g} - \boldsymbol{x_{s,i}}\right) = \begin{cases} 1, & \left(\boldsymbol{x_g} - \boldsymbol{x_{s,i}}\right) = 0 \\ 0, & \left(\boldsymbol{x_g} - \boldsymbol{x_{s,i}}\right) \neq 0 \end{cases} \quad (7)$$

Function $\delta = f(\boldsymbol{x} - \boldsymbol{x_{s,i}})$ ensures selective occurrence of interphase interactions ($\boldsymbol{F}_{\mathbf{exchange}}$ forces) by limiting them to discrete points of space x in the continuous phase, in which the particles of the dispersed phase are present.

The momentum transfer between the gas stream and a single solid particle for the Eulerian-Lagrangian approach is calculated from the following equations (WACHEM, ALMSTEDT 2003):

$$F_{\text{exchange},i} = \frac{18\ \eta\ C_D\ \text{Re}}{\rho_s d_s^2 24}\left(u_g - u_{s,i}\right) \quad (8)$$

$$\text{Re} = \frac{\rho_g d_s |u_g - u_{s,\,i}|}{\eta} \quad (9)$$

Symbols appearing in the above formulas indicate respectively: ρ_s, ρ_g, η, d_s – particle density, fluid density, dynamic fluid viscosity and particle diameter, Re – relative Reynolds number, $\boldsymbol{u_g}$, $\boldsymbol{u_{s,i}}$ – velocity of gas stream and i-th particle. The last element is C_D drag coefficient. The model developed by MORSI and ALEXANDER (1972) for spherical particles was chosen for its calculation (according to the manufacturer's data, the sphericity of circulating particles is 0.95):

$$C_D = a_1 + \frac{a_2}{\mathrm{Re}} + \frac{a_3}{\mathrm{Re}^2} \tag{10}$$

The constant a take different values in the function of the relative Reynolds number. It is one of the most complete correlations, taking into account the wide range of Reynolds numbers used.

Equations describing the movement of the dispersed phase are based on Newton's second law of dynamics. The effects of gravity, interaction with the continuous phase and collisions with walls were taken into account in the calculations (WACHEM, ALMSTEDT 2003):

$$m_s \boldsymbol{a_s} = m_s \boldsymbol{g} + V_s \nabla \boldsymbol{\tau_g} - V_s \nabla P + m_s \boldsymbol{F_{\mathbf{exchange}}} \tag{11}$$

where:

$\boldsymbol{a_s}$ – symbolizes the acceleration of a given solid particle,
V_s – the volume of the particle,
P – the local value of the pressure field,
$\boldsymbol{\tau_g}$ – the stress tensor for the continuous phase, averaged in the calculation cell.

The expression $V_s \nabla \boldsymbol{\tau_g}$ is often omitted due to the small value in comparison with other parts on the right side of the equation. $\boldsymbol{F_{\mathbf{exchange}}}$ is calculated from equation (8). Equation (11) does not contain the term related to the interaction between particles, because it can be omitted in our case due to the low concentration of the dispersed phase.

Inside the modelled apparatus oblique impacts take place (Fig. 3). In order to describe them the normal and tangential restitution coefficients are required. On their basis, the velocity of the particle and the angle of reflection after collision with the wall are determined according to equation (1). The oblique collision of a particle with the wall is schematically presented in Figure 3. The most important parameters of the model are marked on it: oblique incident velocity $\boldsymbol{V_i}$, being the resultant of the normal V_{ni} and tangential V_{ti} component, as well as incidence angles θ_i and critical angle θ_{cr}, the significance of which will be explained later. When particles come into contact with the wall, restitution coefficients e_n, e_t are calculated, leading to the formation of rebound velocity components V_{nr}, V_{tr} and determining the new velocity $\boldsymbol{V_r}$ of the particle after collision.

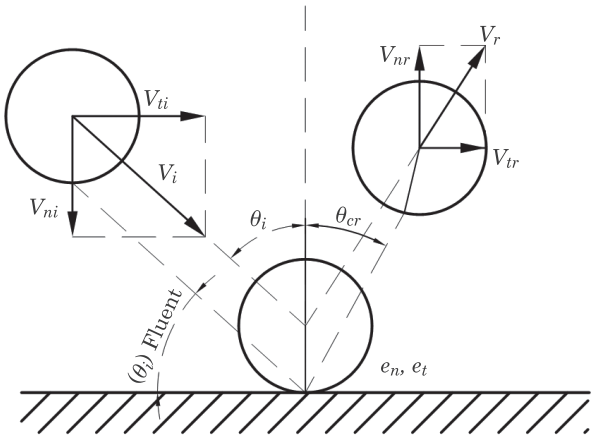

Fig. 3. The oblique impact of sphere on the flat surface
Source: based on LUDWIG and PŁUSZKA (2018).

Calculation of the normal restitution coefficient

Elastic collisions for low particles velocities were described using Hertz theory (TIMOSHENKO, GOODIER 1951). They are characterized by the occurrence of stress wave effect, which is propagating in the material. The propagation of impact takes place at the expense of part of its initial kinetic energy. This dissipated fraction of energy is described using the kinetic energy loss ratio λ, which is correlated with a normal restitution coefficient (WU et al. 2005):

$$e_{n,\text{elast}} = \left(1 - \frac{\lambda}{100}\right)^{1/2} \tag{12}$$

where index elast indicates the range of elastic collisions and λ is calculated from the equation:

$$\lambda = 0.73\ V_{ni}^{3/5} \tag{13}$$

As the collision velocity increases, the significance of plastic interactions also increases, while the significance of elastic interactions is reduced. In this work the analytical dependence of the normal restitution coefficient derived by Thornton from the simplified model of elastoplastic collision was used (THORTON et al. 2001):

$$e_{n,\text{ Thornton}} = \left\{\left(\frac{6\sqrt{3}}{5}\right)\left[1 - \frac{1}{6}\left(\frac{V_y}{V_{ni}}\right)^2\right]\right\}^{1/2}\left\{\left(\frac{V_y}{V_{ni}}\right)\left[\left(\frac{V_y}{V_{ni}}\right) + 2\sqrt{1.2 - 0.2\left(\frac{V_y}{V_{ni}}\right)^2}\right]\right\}^{1/4} \tag{14}$$

where V_y is the yield velocity calculated from relation:

$$V_y = 3.194 \left(\frac{Y^5 \, (R^*)^3}{E^{*4} \, m^*} \right)^{0.5} \tag{15}$$

where Y is the yield strength, R^*, E^*, m^* are the effective radius, Young's modulus and mass for impact of two materials. When the normal component of the particle velocity hitting the wall is greater than V_y, an elastoplastic collision is present and the normal restitution coefficient is calculated from equation (14). Otherwise, an elastic collision occurs and equation (12) is used.

In particle collisions with the deflector in the apparatus under investigation, the model for the normal velocity component will be predominant. In the case of rebounds from the inner surface of the draft tube and two surfaces of the annular zone, the hydrodynamics of the particles will be influenced mainly by the tangential model, which is described below.

Calculation of the tangential restitution coefficient

As with the normal restitution coefficient, the tangential part of the model is described by a single analytical equation. On the basis of available literature it was found that only one model of tangential collisions, presented in the article by WU et al. (2009) can be implemented in a relatively simple way in calculations. Its additional advantage is good correlation with experimental data, which is proved by the authors. Equations (16)–(18) present the most important model formulas (WU et al. 2009):

$$e_t = \begin{cases} 1 - \dfrac{2}{\Theta}[c_1 + c_2 \tanh(c_3 + c_4 \Theta)], & \Theta < \Theta_{\text{crit}} \\ 1 - \dfrac{2}{\Theta}, & \Theta \geq \Theta_{\text{crit}} \end{cases} \tag{16}$$

$$\Theta = \frac{2}{(1 + e_n)\mu} \tan(90° - \theta_i) \tag{17}$$

$$\Theta_{\text{crit}} = \frac{7\kappa - 1}{\kappa} \tag{18}$$

where:

e_n – the normal restitution coefficient (determined by the normal model equation),

μ – the friction coefficient,

κ – the rigidity coefficient and θ is the incident angle.

In this paper θ is defined as the angle between the velocity vector and the wall plane, as opposed to the definition from the source article, where the angle formed by the velocity vector and the normal to the wall plane is operated (Fig. 3). The c coefficients from equation (16) were determined by approximation of the results of numerical simulations of FEM (Finite Element Method) presented in the paper of WU et al. (2009) and amount to: c_1=0.4459, c_2=–0.6112, c_3=0.9288, c_4=–0.4050, respectively.

Materials used in simulations

In order to use the equations presented in the previous chapter, the value of V_y from equation (14) has to be determined. In this case the physical properties of the colliding particles and walls (glass and aluminium) (Tab. 1) must be known (LUDWIG, PŁUSZKA 2018). In the simulations Cellets® 1000 particles produced from microcrystalline cellulose by SYNTHAPHARM were modelled. They are frequently used as drug carrier in the pharmaceutical industry.

Air parameters were assumed to be constant: density 1.22 kg/m^3, kinematic viscosity $1.75 \cdot 10^{-5}$ Pa-s.

Table 1

Physical properties of materials used in simulations

Quantity	Value
Young's modulus for Cellets® C1000 [GPa]	1.559
Young's modulus for borosilicate glass 3.3 [GPa]	64
Young's modulus for aluminium 2017 [GPa]	73
Poisson's ratio for Cellets® C1000	0.3
Poisson's ratio for borosilicone glass 3.3	0.2
Poisson's ratio for aluminium 2017	0.334
Plasticization Pressure for Cellets® C1000 [MPa]	108.55
Yield velocity [m/s]	2.08
Particle density [kg/m^3]	1,570
Particle diameter [mm]	1.11

Model solution

In order to solve the presented model Ansys Fluent solver was used which settings are presented in Table 2 and 3. In the course of previous studies, an optimal numerical mesh with polyhedral cells and the following parameters has been obtained: number of cells 708,621, number of faces 3,968,399, number

Table 2

Model parameters – fluid (continuous) phase

Parameter	Value
Solver	3D, pressure based, steady
Pressure-velocity coupling	SIMPLE
Turbulence model	standard k-ε with modification "realizable"
Description of near-wall zone	enhanced wall treatment
Boundary condition at the inlet to column	velocity inlet
Boundary condition at the outlet of column	pressure outlet
Discretization scheme	second order upwind
Limit of scaled residuals	$1 \cdot 10^{-4}$

Table 3

Model parameters – particles (discrete phase)

Parameter	Value
Type of solver	transient, interaction with continuous phase
Number of continuous phase iterations on one iteration of discrete phase	10
Type of injection surface	surface
Particle diameter distribution type	uniform
Injection time	10^{-1} s
Number of particle in parcel	varying with the mass of the bed
Wall boundary condition	reflect

of nodes 2,967,161, maximal skewness 0.583836 (LUDWIG, ZAJĄC 2017, LUDWIG, PŁUSZKA 2018). The flow was assumed as isothermic and incompressible.

During the simulation, only the air outflow from the main spouting nozzle was taken into account, which was determined on the basis of experimental observations of the bed (Tab. 4) (LUDWIG, ZAJĄC 2017). The results of the average particle velocity for different values of friction coefficient (0.1–0.4) and volumes of the poured bed (100–400 cm^3) were read in each calculation time step from a cross-section located approximately in the middle of the upper segment (Fig. 4).

Table 4

Air velocities in the spouting nozzle corresponding to various volumes of bed applied during calculations

w_0 [m/s]	V_{bed} [cm^3]	H_{bed} [mm]
189	100	34
278	200	54
333	300	74
407	400	94

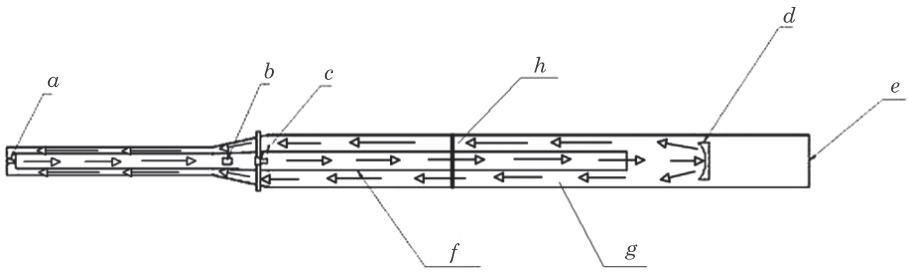

Fig. 4. Section of the simplified apparatus geometry used in the simulation (arrows show the circulation of particles): *a* — spouting air nozzle, *b* — powder spraying nozzle, *c* — liquid spraying nozzle, *d* — deflector, *e* — air outlet, *f* — draft tube, *g* – annular zone, *h* – localization of measurements and simulation data reading
Source: based on LUDWIG and PŁUSZKA (2018).

These results were then averaged over time. The averaged value of particle velocity was compared with experimental results obtained by PIV (Particle Image Velocimetry) method, which was described in detail in the article of LUDWIG and ZAJĄC (2017).

Results and discussion

In the course of calculations, a relatively small influence of friction coefficient on particles velocity was observed in the tested zones of the apparatus. Its increase by 300% from 0.1 to 0.4 caused an increase in particles velocity in the draft tube by maximum 16% (on average 14%) (Fig. 5), while its decrease in the annular zone by maximum 25% (on average 18%) (Fig. 6). The changes were

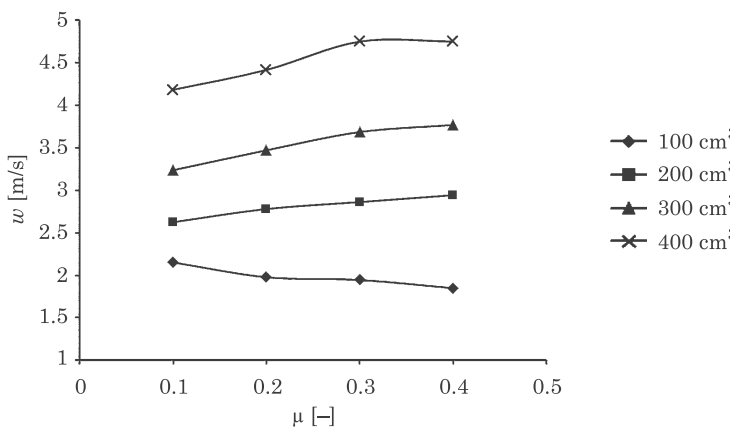

Fig. 5. Particles velocity in the draft tube as a function of friction coefficient for different volumes of the bed

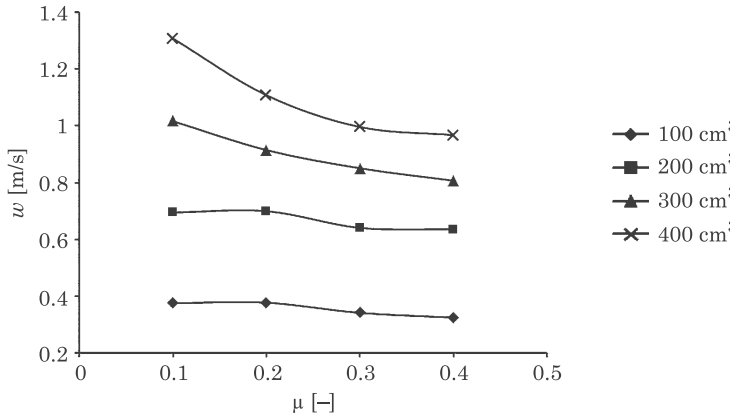

Fig. 6. Particles velocity in the annular zone as a function of friction coefficient for different volumes of the bed

most visible for large volumes of the bed in the annulus. For V_{bed}=100 cm^3 and V_{bed}=400 cm^3 they equalled respectively –13% and –26% in this zone (Fig. 6). In the draft tube the influence of the number of circulating particles was small (for V_{bed} = 200 cm^3 the change was 12% and for V_{bed} =400 cm^3 13%) (Fig. 5).

As the volume of the bed increases, the number of collisions between particles and the walls of the device increases. The number of collisions in the annulus is much higher than in the draft tube because the particles after rebounding from the curved bowl of the deflector move on curvilinear tracks, rebounding successively from the outer wall of the draft tube and the inner wall of the apparatus (LUDWIG, PŁUSZKA 2018). Inside the draft tube, except in the zone just above the spouting gas nozzle where there is intensive mixing, the bed moves parallel to the walls of the device.

The different dependency of particle velocity on the friction coefficient in the draft tube and the annular zone results from the properties of equation (15) (Fig. 7). According to it, in the area of low test angles (below approximately 70°, depending on the normal restitution coefficient), an increase in the value of the friction coefficient causes a decrease in the tangential restitution coefficient. For high incidence angles this relationship is reversed. A relatively small number of collisions with a high incidence angle occur in the draft tube, especially in the bottom part of the apparatus, where the bed is intensively circulating (LUDWIG, PŁUSZKA 2018). In the annular zone, on the other hand, the collisions are more frequent and the particles collide with the walls at low angles.

In the case of a 100 cm^3 bed, the particle velocity in both the draft tube and the annular zone always decreases with the increase in the friction coefficient from 0.1 to 0.4, but this change is small and amounts to –13% and –14% respectively (Fig. 5 and 6). With such a small number of particles, they do not mix in the lower zone of the draft tube and they move parallel to the walls from

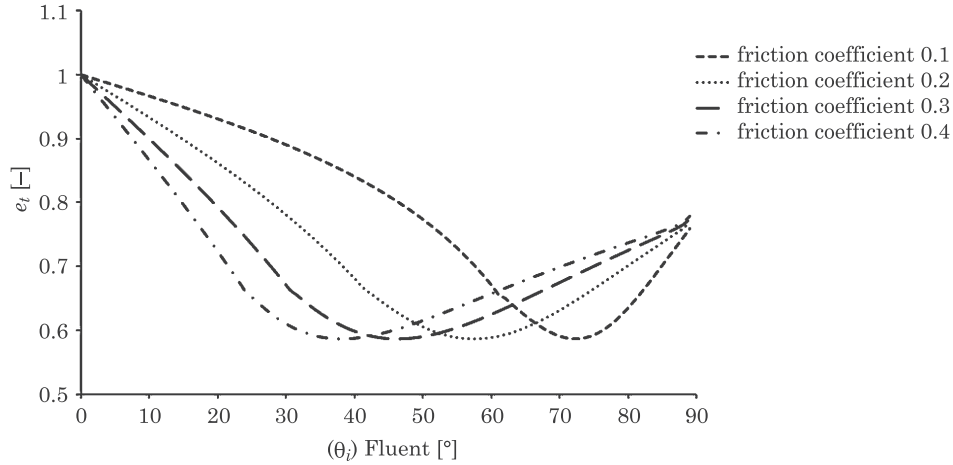

Fig. 7. Tangential restitution coefficient as a function of incident angle between particle velocity vector and the wall plane for different friction coefficients according to equation (16) (normal restitution coefficient 0.9)

the beginning and their incidence angles are small, resulting in a decrease in tangential restitution coefficients as the friction coefficient increases.

The curve of particle velocity simulation results in the draft tube for the coefficient of friction 0.1 gives the highest accuracy in reference to the experimental data in the draft tube (the largest and smallest relative errors are 15% and 1% respectively) and in the annular zone (the largest and smallest relative errors are 57% and 34% respectively) (Fig. 8 and 9). However, the increase in accuracy with respect to the value of 0.2 used in the previous calculations is small. In this case, the largest and smallest relative errors in the draft tube were 22% and 1% respectively and in the annular zone 57% and 44%. The relative error

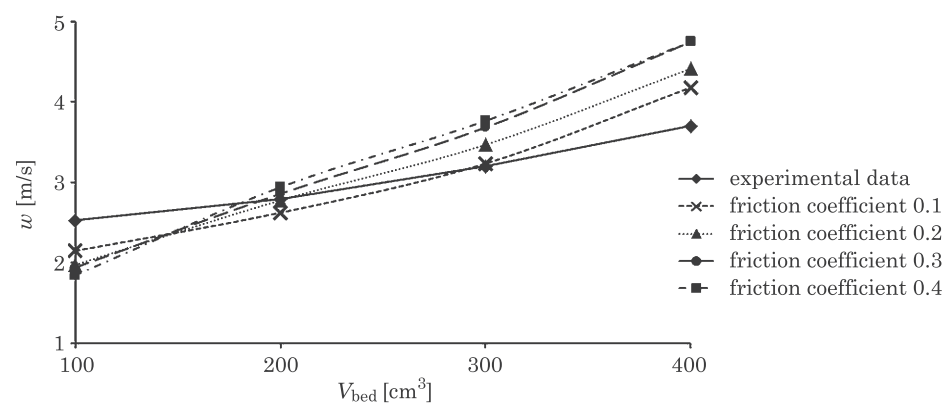

Fig. 8. Particles velocity as a function of bed's volume for different friction coefficients in the draft tube

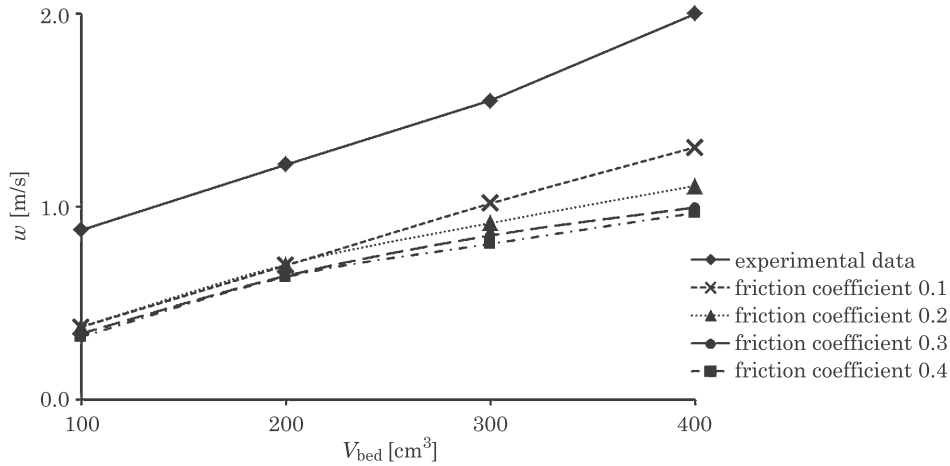

Fig. 9. Particles velocity as a function of bed's volume for different friction coefficients in the annular zone

in the annular zone remained relatively high, which was related to the hydrodynamics of the bed flow at this point (high values of the normal component of the particle velocity) and the properties of Thorton's equation (rapid decrease in the normal restitution coefficient with an increase in incident velocity). In turn, high values of incidence angles of particles against the apparatus walls in this zone caused a decrease in the tangential restitution coefficient. Both these factors caused the calculated particle velocity to be understated. A detailed description of this mechanism can be found in article LUDWIG and PŁUSZKA (2018).

Conclusions

The paper analyses the impact of the friction coefficient, difficult to measure and therefore not widely published in the literature, on the results of particle velocity simulation in a spout-fluid bed apparatus for dry coating. The most important zones from the point of view of the process have been taken into account: the draft tube and the annulus. It has been shown that even a large change in the assumed value of the friction coefficient of particles against the wall does not significantly affect the accuracy of model calculations. Therefore, this value does not need to be determined experimentally with high accuracy, which is very difficult. For model calculations it is enough to know only the approximate value of this parameter. An apparently surprising observation was also made that, depending on the particle incidence angle, an increase in the friction coefficient may cause both an increase and a decrease in their velocity. The choice of models calculating perpendicular and tangential restitution

coefficients has a significantly greater influence than the friction coefficient value. The literature offers many items concerning the description of these correlations (LI et al. 2001, JACKSON et. al. 2010). This will be the subject of my further research.

Acknowledgements

The studies were funded by the Polish National Science Centre within the framework of the research grant UMO-2013/09/B/ST8/00157.

References

CUNDALL P.A., STRACK O.D. 1979. *A discrete element model for granular assemblies*. Géotechnique, 29: 47–65.

DEEN N.G., SINT ANNALAND M. VAN, HOEF M.A. VAN DER, KUIPERS J.A.M. 2007. *Review of discrete particle modeling of fluidized beds*. Chemical Engineering Science, 62: 28–44.

EPSTEIN N., GRACE J.R. 2011. *Spouted and Spout-Fluid Bed. Fundamentals and Application*. Cambridge University Press, Cambridge.

GELDART D. 1973. *Types of fluidization*. *Powder Technology*, 7: 285–292.

HOOMANS B.P.B., KUIPERS J.A.M., BRIELS W.J., SWAAIJ W.P.M. VAN. 1996. *Discrete particle simulation of bubble and slug formation in a two-dimensional gas-fluidised bed: a hard-sphere approach*. Chemical Engineering Science, 51: 99–118.

ISHIKURA T., NAGASHIMA H., IDE M. 2003. *Hydrodynamics of a spouted bed with a porous draft tube containing a small amount of finer particles*. Powder Technology, 131: 56–65.

JACKSON R.L., GREEN I., MARGHITU D.B. 2010. *Predicting the coefficient of restitution of impacting elastic-perfectly plastic spheres*. Nonlinear Dynamics, 60: 217–229.

JAWORSKI Z. 2005. *Computational fluid dynamics in chemical and process engineerin*. First ed. EXIT, Warszawa.

KARLSSON S., BJOERN I.N., FOLESTAD S., RASMUSON A. 2006. *Measurements of the particle movement in the fountain region of a Wurster type bed*. Powder Technology, 165: 22–29.

LI L.Y., WU C.Y., THORNTON C. 2002. *A theoretical model for the contact of elastoplastic bodies. Proceedings of the Institution of Mechanical Engineers*. Part C. Journal of Mechanical Engineering Science, 216: 421–431.

LUDWIG W. 2016. *Hydrodynamics of particles flow in the modified Wurster apparatus operating in a fast circulating dilute spout-fluid bed regime*. In Proceedings of the 22nd Polish Conference of Chemical and Process Engineering in Spala, p. 788–799.

LUDWIG W., PŁUSZKA P. 2018. *Euler-Lagrange model of particles circulation in a spout-fluid bed apparatus for dry coating*. Powder Technology, 328: 375–388.

LUDWIG W., ZAJĄC D. 2017. *Modeling of particle velocities in an apparatus with a draft tube operating in a fast circulating dilute spout-fluid bed regime*. Powder Technology, 319: 332–345.

MATHUR K.B., GISHLER P.E. 1955. *A technique for contacting gases with coarse solid particles*. AICHE Journal, 1: 157–164.

MOLINER C., MARCHELLI F., BOSIO B., ARATO E. 2017. *Modelling of Spouted and Spout-Fluid Beds: Key for Their Successful Scale Up*. Energies, 10: 1729–1768.

MORSI S.A., ALEXANDER A.J. 1972. *An Investigation of Particle Trajectories in Two-Phase Flow Systems*. Journal of Fluid Mechanics, 55: 193–208.

RANADE V.V. 2002. *Computational Flow Modeling for Chemical Reactor Engineering*. Vol. 5. First ed. Academic Press, San Diego.

SUTKAR V.S., DEEN N.G., KUIPERS J.A.M. 2013. *Spout fluidized beds: recent advances in experimental and numerical studies*. Chemical Engineering Science, 86: 124–136.

SZAFRAN R.G., LUDWIG W., KMIEĆ A. 2012. *New spout-fluid bed apparatus for electrostatic coating of fine particles and encapsulation*. Powder Technology, 225: 52–57.

TEUNOU E., PONCELET D. 2002. *Batch and continuous bed coating — review and state of the art*. Journal of Food Engineering, 53: 325–340.

THORNTON C., NING Z., WU C.Y, NASRULLAH M., LI L.Y. 2001. *Contact Mechanics and Coefficients of Restitution*. Granular Gases, Springer, Berlin, p. 184–194.

TIMOSHENKO S. , GOODIER J.N. 1951. *Theory of Elasticity*. Second ed. McGraw-Hill, New York.

TSUJI Y., KAWAGUCHI T., TANAKA T. 1993. *Discrete particle simulation of two-dimensional fluidized bed*. Powder Technology, 77: 79–87.

WACHEM B.G.M. ALMSTEDT A.E. 2003. *Methods for multiphase computational fluid dynamics*. Chemical Engineering Journal, 96: 81–98.

WU C.Y, LI L.Y., THORNTON C. 2005. *Energy dissipation during normal impact of elastic and elastic-plastic spheres*. International Journal of Impact Engineering, 32: 593–604.

WU C.Y., SEVILLE J. 2016. *Particle Technology and Engineering*. Elsevier.

WU C.Y., THORNTON C., LI L.Y. 2009. *A semi-analytical model for oblique impacts of elastoplastic spheres*. Proceedings of the Royal Society, A, 465: 937–960.

ZHONG W., ZHANG Y., JIN B. 2010. *Novel method to study the particle circulation in a flatbottom spout-fluid bed*. Energy & Fuels, 24: 5131–5138.